6160 *Inorg. Chem.* **2010**, *49*, 6160–6171
DOI: 10.1021/ic100817s

Inorganic Chemistry
Article

Experimental and Computational Study of the Structural and Electronic Properties of Fe^{II}(2,2′-bipyridine)$(mes)_2$ and $[Fe^{II}$(2,2′-bipyridine)$(mes)_2]^-$, a Complex Containing a 2,2′-Bipyridyl Radical Anion

Mark Irwin,[†] Rhiannon K. Jenkins,[†] Mark S. Denning,[†] Tobias Krämer,[†] Fernande Grandjean,[‡] Gary J. Long,*[,§] Radovan Herchel,[∥] John E. McGrady,*[,†] and Jose M. Goicoechea*[,†]

[†]*Department of Chemistry, Inorganic Chemistry Laboratory, University of Oxford, South Parks Road, Oxford OX1 3QR, U.K.,* [‡]*Department of Physics, B5, University of Liège, B-4000, Sart-Tilman, Belgium,* [§]*Department of Chemistry, Missouri University of Science and Technology, University of Missouri, Rolla, Missouri 65409-0010, and* [∥]*Department of Inorganic Chemistry, Faculty of Science, Palacký University, tr. 17. Listopadu 12, 77146 Olomouc, Czech Republic*

Received April 26, 2010

Addition of potassium metal and 2,2,2-crypt (4,7,13,16,21,24-hexaoxa-1,10-diazabicyclo[8.8.8]hexacosane) to a tetrahydrofuran (THF) solution of Fe(2,2′-bipyridine)$(mes)_2$ (**1**; mes = 2,4,6-$Me_3C_6H_2$) yielded the anionic complex $[Fe$(2,2′-bipyridine)$(mes)_2]^-$ which was isolated as [K(2,2,2-crypt)][Fe(2,2′-bipyridine)$(mes)_2$] (**2**) alongside the side-product $[K$(2,2,2-crypt)$][Fe(mes)_3]\cdot C_6H_{12}$ (**3**). A compositionally pure sample of **2** was obtained by dissolving a mixture of **2** and **3** in dry pyridine and layering the resulting solution with toluene. Solid state magnetic susceptibility measurements on **1** reveal Curie−Weiss paramagnetic behavior with a molar magnetic moment of 5.12(1) μ_B between 20 and 300 K, a value which is in line with the expected iron(II) spin-only value of 4.90 μ_B. The magnetic measurements carried out on **2** reveal more complex temperature dependent behavior consistent with intramolecular antiferromagnetic coupling ($J = -46$ cm^{-1}) between the unpaired electrons of the iron(II) ion ($S_{Fe}=2$) and a π^* orbital of the bipyridyl radical (S_{bipy} = 1/2). Structural data, Mössbauer and electron paramagnetic resonance (EPR) spectroscopic measurements, and density functional theory (DFT) calculations are all consistent with this model of the electronic structure. To the best of our knowledge, species **2** represents the first crystallographically characterized transition metal complex of the 2,2′-bipyridyl ligand for which magnetic, spectroscopic, and computational data indicate the presence of an unpaired electron in the π^* antibonding orbital.

Introduction

Transition metal complexes of open-shell ("non-innocent") ligands have been extensively studied in recent years because they can often exhibit unusual reactivity when compared to their closed-shell analogues.[1,2] Moreover, increased access to modern electron paramagnetic resonance (EPR) spectrometers and superconducting quantum interference device (SQUID) magnetometers has facilitated the analysis of their electronic structures making the study of such species more accessible. Many transition metal complexes of radical organic ligands are believed to be key intermediates in catalysis or important biological processes such as enzyme-catalyzed transformations, making the understanding of their electronic structure of fundamental importance.[3,4]

Perhaps the most extensively studied transition metal complexes of radical anions are those of semiquinone and phenoxyl radicals.[5,6] Other ligand systems which exhibit non-innocent behavior include species such as dithiolates,[7] α-diimines,[8] α-iminopyridines,[9] α-iminoketones,[10] tetrazenes,[11] and imino- and thio-phenolates.[12] Recently, the first family of aminyl radical complexes was also reported in the chemical literature.[13] Attributing definitive oxidation states to metal centers and ligands in these systems presents a significant

*To whom correspondence should be addressed. E-mail: glong@mst.edu (G.J.L.); john.mcgrady@chem.ox.ac.uk (J.E.McG.); jose.goicoechea@chem.ox.ac.uk (J.M.G.).

(1) Kaim, W. *Coord. Chem. Rev.* **1987**, *76*, 187, and references reported therein.
(2) (a) Hendrickson, D. N.; Pierpont, C. G. In *Spin Crossover in Transition Metal Compounds II*; Springer: Berlin, London, 2004; Vol. *234*, p 63. (b) Pierpont, C. G.; Lange, C. W. *Prog. Inorg. Chem.* **1994**, *41*, 331.
(3) (a) Grützmacher, H. *Angew. Chem., Int. Ed.* **2008**, *47*, 1814. (b) Ray, K.; Petrenko, T.; Wieghardt, K.; Neese, F. *Dalton Trans.* **2007**, 1552. (c) Knijnenburg, Q.; Gambarotta, S.; Budzelaar, P. H. M. *Dalton Trans.* **2006**, 5442. (d) Bouwkamp, M. W.; Bowmann, A. C.; Lobkovsky, E.; Chirik, P. J. *J. Am. Chem. Soc.* **2006**, *128*, 13340.
(4) (a) Frey, P. A. *Chem. Rev.* **1990**, *90*, 1343. (b) Whittaker, J. W. *Chem. Rev.* **2003**, *103*, 2347. (c) Jazdzewski, B. A.; Tolman, W. B. *Coord. Chem. Rev.* **2000**, *200−202*, 633. (d) Dooley, D. M.; McGuirl, M. A.; Brown, D. E.; Turowski, P. N.; McIntire, W. S.; Knowles, P. F. *Nature* **1991**, *349*, 262.

 Published on Web 06/09/2010

challenge, generally requiring extensive magnetic and spectroscopic data. As a result, many examples of ligands exhibiting non-innocent behavior can go unidentified. Recent studies by our research group have prompted us to probe the electronic structure of bipyridyl complexes of low-valent transition metals in search of evidence for non-innocent behavior in this ubiquitous ligand.

It has long been established that the chemical reduction of 2,2′-bipyridine (2,2′-bipy) can give rise to the 2,2′-bipyridyl radical anion and dianion,[14−16] and a number of well-defined coordination complexes of the 2,2′-bipyridyl radical have been reported in the field of lanthanide coordination chemistry.[17] Research on homoleptic first-row transition metal complexes of 2,2′-bipy first highlighted the possibility of bipyridyl radical coordination to transition metal ions and several examples have now been spectroscopically characterized via EPR, IR, electronic and/or resonance Raman measurements. There remains, however, a lack of definitive structural data for complexes of this type: a survey of crystallographically characterized low-valent transition metal complexes of 2,2′-bipyridine reveals several systems in which bond metric parameters hint at the possibility of radical (or even dianionic) character,[18,19] but interpretation of this structural data is ambiguous, simply because a one-electron reduction of the ligand has the same qualitative effect as enhanced π-backbonding from a reduced metal center. Both result in population of the lowest unoccupied molecular orbital (LUMO) of 2,2′-bipy and hence contraction of the C−C bond linking the two rings (vide infra). Subsequently, in the absence of magnetic data it is difficult to distinguish the two mechanisms. To the best of our knowledge, there are no transition metal complexes of the 2,2′-bipyridyl radical where structural, spectroscopic, and magnetic data are available to establish an unequivocal assignment of oxidation states.

Herein we report the isolation and electronic characterization of [K(2,2,2-crypt)][Fe(2,2′-bipyridine)(mes)$_2$] (**2**), along with its neutral parent compound Fe(2,2′-bipyridine)(mes)$_2$ (**1**) and apply single-crystal X-ray diffraction, Mössbauer and EPR spectroscopy, SQUID magnetometry, and density functional theory (DFT) to characterize their electronic structures. All of these physiochemical measurement are consistent with the presence of a 2,2′-bipyridyl radical anion

(5) (a) Evangelio, E.; Ruiz-Molina, D. *Eur. J. Inorg. Chem.* **2005**, 2957. (b) Rijnberg, E.; Richter, B.; Thiele, K. H.; Boersma, J.; Veldman, N.; Spek, A. L.; van Koten, G. *Inorg. Chem.* **1998**, *37*, 56. (c) Khusniyarov, M. M.; Harms, K.; Burghaus, O.; Sundermeyer, J. *Eur. J. Inorg. Chem.* **2006**, 2985. (d) Gardiner, M. G.; Hanson, G. R.; Henderson, M. J.; Lee, F. C.; Raston, C. L. *Inorg. Chem.* **1994**, *33*, 2456. (e) Lange, C. W.; Conklin, B. J.; Pierpont, C. G. *Inorg. Chem.* **1994**, *33*, 1276. (f) Attia, A. S.; Pierpont, C. G. *Inorg. Chem.* **1997**, *36*, 6184. (g) Sato, O.; Cui, A.; Matsuda, R.; Tao, J.; Hayami, S. *Acc. Chem. Res.* **2007**, *40*, 361. (h) Ohtsu, H.; Tanaka, K. *Angew. Chem., Int. Ed.* **2004**, *43*, 6301.

(6) Chaudhuri, P.; Wieghardt, K. *Prog. Inorg. Chem.* **2001**, *50*, 151.

(7) (a) Wang, K.; Stiefel, E. I. *Science* **2001**, *291*, 106. (b) Harrison, D. J.; Nguyen, N.; Lough, A. J.; Fekl, U. *J. Am. Chem. Soc.* **2006**, *128*, 11026. (c) Kapre, R.; Bothe, E.; Weyhermüller, T.; George, S. D.; Wieghardt, K. *Inorg. Chem.* **2007**, *46*, 5642. (d) Kapre, R.; Ray, K.; Sylvestre, I.; Weyhermüller, T.; George, S. D.; Neese, F.; Wieghardt, K. *Inorg. Chem.* **2006**, *45*, 3499. (e) Ray, K.; George, S. D.; Solomon, E. I.; Wieghardt, K.; Neese, F. *Chem.—Eur. J.* **2007**, *13*, 2783. (f) Ray, K.; Begum, A.; Weyhermüller, T.; Piligkos, S.; Van Slageren, J.; Neese, F.; Wieghardt, K. *J. Am. Chem. Soc.* **2005**, *127*, 4403. (g) Ray, K.; Bill, E.; Weyhermüller, T.; Wieghardt, K. *J. Am. Chem. Soc.* **2005**, *127*, 5641. (h) Ray, K.; Weyhermüller, T.; Neese, F.; Wieghardt, K. *Inorg. Chem.* **2005**, *44*, 5345. (i) Patra, A. K.; Bill, E.; Weyhermüller, T.; Stobie, K.; Bell, Z.; Ward, M. D.; McCleverty, J. A.; Wieghardt, K. *Inorg. Chem.* **2006**, *45*, 6541. (j) Petrenko, T.; Ray, K.; Wieghardt, K.; Neese, F. *J. Am. Chem. Soc.* **2006**, *128*, 4422. (k) Szilagyi, R. K.; Lim, B. S.; Glaser, T.; Holm, R. H.; Hedman, B.; Hodgson, K. O.; Solomon, E. I. *J. Am. Chem. Soc.* **2003**, *125*, 9158. (l) Ray, K.; Weyhermüller, T.; Goossens, A.; Crajé, M. W. J.; Wieghardt, K. *Inorg. Chem.* **2003**, *42*, 4082.

(8) (a) De Bruin, B.; Bill, E.; Bothe, E.; Weyhermüller, T.; Wieghardt, K. *Inorg. Chem.* **2000**, *39*, 2936. (b) Dutta, S. K.; Beckmann, U.; Bill, E.; Weyhermüller, T.; Wieghardt, K. *Inorg. Chem.* **2000**, *39*, 3355. (c) Muresan, N.; Chopek, K.; Weyhermüller, T.; Neese, F.; Wieghardt, K. *Inorg. Chem.* **2007**, *46*, 5327. (d) Muresan, N.; Weyhermüller, T.; Wieghardt, K. *Dalton Trans.* **2007**, 4390. (e) Chopek, K.; Bill, E.; Ueller, T. W.; Wieghardt, K. *Inorg. Chem.* **2005**, *44*, 7087. (f) Blanchard, S.; Neese, F.; Bothe, E.; Bill, E.; Weyhermüller, T.; Wieghardt, K. *Inorg. Chem.* **2005**, *44*, 3636.

(9) (a) Lu, C. C.; Bill, E.; Weyhermüller, T.; Bothe, E.; Wieghardt, K. *J. Am. Chem. Soc.* **2008**, *130*, 3181. (b) Wile, B. M.; Trovitch, R. J.; Bart, S. C.; Tondreau, A. M.; Lobkovsky, E.; Milsmann, C.; Bill, E.; Wieghardt, K.; Chirik, P. J. *Inorg. Chem.* **2009**, *48*, 4190.

(10) Lu, C. C.; Bill, E.; Weyhermüller, T.; Bothe, E.; Wieghardt, K. *Inorg. Chem.* **2007**, *46*, 5347.

(11) Cowley, R. E.; Bill, E.; Neese, F.; Brennessel, W. W.; Holland, P. L. *Inorg. Chem.* **2009**, *48*, 4828.

(12) (a) Blackmore, K. J.; Lal, N.; Ziller, J. W.; Heyduk, A. F. *J. Am. Chem. Soc.* **2008**, *130*, 2728. (b) Haneline, M. R.; Heyduk, A. F. *J. Am. Chem. Soc.* **2006**, *128*, 8410. (c) Chun, H.; Verani, C. N.; Chaudhuri, P.; Bothe, E.; Bill, E.; Weyhermüller, T.; Wieghardt, K. *Inorg. Chem.* **2001**, *40*, 4157. (d) Chaudhuri, P.; Verani, C. N.; Bill, E.; Bothe, E.; Weyhermüller, T.; Wieghardt, K. *J. Am. Chem. Soc.* **2001**, *123*, 2213. (e) Verani, C. N.; Gallert, S.; Bill, E.; Weyhermüller, T.; Wieghardt, K.; Chaudhuri, P. *Chem. Commun.* **1999**, 1747. (f) Chun, M.; Weyhermüller, T.; Bill, E.; Wieghardt, K. *Angew. Chem., Int. Ed.* **2001**, *40*, 2489. (g) Kokatam, S.; Weyhermüller, T.; Bothe, E.; Chaudhuri, P.; Wieghardt, K. *Inorg. Chem.* **2005**, *44*, 3709. (h) Bachler, V.; Olbrich, G.; Neese, F.; Wieghardt, K. *Inorg. Chem.* **2002**, *41*, 4295. (i) Ghosh, P.; Begum, A.; Bill, E.; Weyhermüller, T.; Wieghardt, K. *Inorg. Chem.* **2003**, *42*, 3208. (j) Ghosh, P.; Begum, A.; Herebian, D.; Bothe, E.; Hildenbrand, K.; Weyhermüller, T.; Wieghardt, K. *Angew. Chem., Int. Ed.* **2003**, *42*, 563. (k) Ghosh, P.; Bill, E.; Weyhermüller, T.; Wieghardt, K. *J. Am. Chem. Soc.* **2003**, *125*, 3967. (l) Min, K. S.; Weyhermüller, T.; Wieghardt, K. *Dalton Trans.* **2003**, 1126.

(13) (a) Büttner, T.; Geier, J.; Frison, G.; Harmer, J.; Calle, C.; Schweiger, A.; Schönberg, H.; Grützmacher, H. *Science* **2005**, *307*, 235. (b) Miyazato, Y.; Wada, T.; Muckerman, J. T.; Fujita, E.; Tanaka, K. *Angew. Chem., Int. Ed.* **2007**, *46*, 5728. (c) Mankad, N. P.; Antholine, W. E.; Szilagyi, R. K.; Peters, J. C. *J. Am. Chem. Soc.* **2009**, *131*, 3878.

(14) Creutz, C. *Comments Inorg. Chem.* **1982**, *1*, 293, and references reported therein.

(15) Constable, E. C. Homoleptic Complexes of 2,2′-Bipyridine. In *Advances in Inorganic Chemistry*; Sykes, A. G., Ed.; Academic Press: San Diego, 1989; Vol. *34*, p 1, and references reported therein.

(16) (a) Saito, Y.; Takemoto, J.; Hutchinson, B.; Nakamoto, K. *Inorg. Chem.* **1972**, *11*, 2003. (b) Kawashima, H.; Kato, T.; Shida, T. *J. Raman Spectrosc.* **1991**, *22*, 187. (c) Castellà-Ventura, M.; Kassab, E.; Buntinx, G.; Poizat, O. *Phys. Chem. Chem. Phys.* **2000**, *2*, 4682. (d) Danzer, G. D.; Golus, J. A.; Strommen, D. P.; Kincaid, J. R. *J. Raman Spectrosc.* **1990**, *21*, 3. (e) Bradley, P. G.; Kress, N.; Hornberger, B. A.; Dallinger, R. F.; Woodruff, W. H. *J. Am. Chem. Soc.* **1981**, *103*, 7441. (f) König, E.; Herzog, S. *J. Inorg. Nucl. Chem.* **1970**, *32*, 585. (g) König, E.; Kremer, S. *Chem. Phys. Lett.* **1970**, *5*, 87. (h) Mahon, C.; Reynolds, W. L. *Inorg. Chem.* **1967**, *6*, 1927. (i) Zahlan, A.; Heineken, F. W.; Bruin, M.; Bruin, F. *J. Chem. Phys.* **1962**, *37*, 683. (j) Dos Santos-Veiga, J.; Reynolds, W. L.; Bolton, J. R. *J. Chem. Phys.* **1966**, *44*, 2214. (k) Henning, J. C. M. *J. Chem. Phys.* **1966**, *44*, 2139. (l) Van Voorst, J. D. W.; Zijlstra, W. G.; Sitters, R. *Chem. Phys. Lett.* **1967**, *1*, 321. (m) König, E.; Fischer, H. *Z. Naturforsch.* **1962**, *37*, 683. (n) Kaim, W. *Chem. Ber.* **1981**, *114*, 3789.

(17) (a) Evans, W. J.; Gonzales, S. L.; Ziller, J. W. *J. Am. Chem. Soc.* **1994**, *116*, 2600. (b) Schultz, M.; Boncella, J. M.; Berg, D. J.; Tilley, T. D.; Andersen, R. A. *Organometallics* **2002**, *21*, 460. (c) Walter, M. D.; Berg, D. J.; Andersen, R. A. *Organometallics* **2006**, *25*, 3228. (d) Booth, C. H.; Walter, M. D.; Kazhdan, D.; Hu, Y.-J.; Lukens, W. W.; Bauer, E. D.; Maron, L.; Eisenstein, O.; Andersen, R. A. *J. Am. Chem. Soc.* **2009**, *131*, 6480.

(18) (a) Mootz McPherson, A.; Fieselmann, B. F.; Lichtenberger, D. L.; McPherson, G. L.; Stucky, G. D. *J. Am. Chem. Soc.* **1979**, *101*, 3425. (b) Chisholm, M. H.; Huffman, J. C.; Rothwell, I. P.; Bradley, P. G.; Kress, N.; Woodruff, W. H. *J. Am. Chem. Soc.* **1981**, *103*, 4945. (c) Radonovich, L. J.; Eyring, M. W.; Groshens, T. J.; Klabunde, K. J. *J. Am. Chem. Soc.* **1982**, *104*, 2816. (d) Perez-Cordero, E. E.; Campana, C.; Echegoyen, L. *Angew. Chem., Int. Ed.* **1997**, *36*, 137. (e) Rosa, P.; Mézailles, N.; Richard, L.; Mathey, F.; Le Floch, P. *Angew. Chem., Int. Ed.* **2000**, *39*, 1823. (f) Mork, B. V.; McMillan, A.; Yuen, H.; Tilley, T. D. *Organometallics* **2004**, *23*, 2855.

(19) Lenges, C. P.; White, P. S.; Marshall, W. J.; Brookhart, M. *Organometallics* **2000**, *19*, 1247.

in **2**, and suggest that the unpaired electron of the radical is antiferromagnetically coupled to the transition metal center.

Experimental Section

General Methods. All reactions and product manipulations were carried out under an inert atmosphere employing standard Schlenk-line or glovebox techniques. All solvents (toluene, 99.9%; hexanes, 99.9%; tetrahydrofuran (THF), 99.9%; Rathburn Chemicals, Ltd.) were dried using an MBraun SPS-800 solvent purification system and stored in gastight ampules under argon, with the exception of ethylenediamine (99%, Aldrich) which was distilled over sodium metal. Potassium metal (99.95%, Aldrich) was stored under dinitrogen in an MBraun UNIlab glovebox maintained at <0.1 ppm H_2O and <0.1 ppm O_2 and used as received. 2,2′-Bipyridine ($>99\%$ Acros) and 2,2,2-crypt (4,7,13,16,21,24-hexaoxa-1,10-diazabicyclo[8.8.8]-hexacosane; $\geq$ 99% Merck) were used as delivered after being carefully dried under vacuum. $Fe_2(mes)_4$ (mes = 2,4,6-$Me_3C_6H_2$) was synthesized according to a previously reported literature procedure.[20]

Fe(2,2′-bipyridine)(mes)$_2$ (1). In a typical reaction, 200 mg of $Fe_2(mes)_4$ (0.35 mmol) and 110 mg of 2,2′-bipyridine (0.70 mmol) were dissolved in 5 mL of THF under dinitrogen and stirred for an hour. A deep reddish-purple solution was immediately observable. The resulting solution was filtered and layered with approximately 20 mL of hexanes. The mixture was left to crystallize over several days affording 195 mg of red crystalline Fe(2,2′-bipyridine)$(mes)_2$ (yield 62%). A powder X-ray diffraction pattern was obtained which matched the simulated diffraction pattern based on the single-crystal X-ray diffraction data (Supporting Information, Figure S1). Anal. Calcd for $FeC_{28}H_{30}N_2$: C, 74.65%; H, 6.72%; N, 6.22%. Found: C, 74.52%; H, 6.60%; N, 6.23%. ES+ MS: *m*/*z* 212.1, [Fe(2,2-bipyridine)]$^+$; 331.2, [Fe(mes)(2,2-bipyridine)]$^+$; 368.2, [Fe(2,2-bipyridine)$_2$]$^+$; 450.4, [Fe(mes)$_2$(2,2-bipyridine)]$^+$; 487.4 [Fe(mes)-(2,2-bipyridine)$_2$]$^+$; 524.4 [Fe(2,2-bipyridine)$_3$]$^+$. ES− MS: *m*/*z* 293.2, [Fe(mes)$_2$]$^-$; 413.3, [Fe(mes)$_3$]$^-$. IR (cm^{-1}): 628 (w), 647 (w), 705 (w), 735 (s), 744 (w), 763 (vs), 839 (s), 850 (m), 1012 (s), 1042 (w), 1057 (w), 1101 (w), 1112 (w), 1156 (s), 1166 (w), 1211 (w), 1247 (m), 1278 (w), 1310 (m), 1366 (m), 1392 (m), 1439 (vs), 1470 (m), 1530 (w), 1561 (w), 1571 (w), 1589 (m), 1596 (s), 1599 (s). Raman (cm^{-1}): 96 (w), 140(s), 250 (m), 293 (w), 359 (w), 419 (w), 483 (w), 548 (w), 651 (m), 770 (w), 1016 (s), 1170 (m), 1282 (m), 1315 (s), 1487 (s), 1565 (m), 1599 (w).

[K(2,2,2-crypt)][Fe(2,2′-bipyridine)(mes)$_2$] (2). A 250 mg portion of **1** (0.56 mmol) was reacted with 22 mg of K (0.56 mmol) and 212 mg of 2,2,2-crypt (0.56 mmol) in 5 mL of THF and left to stir overnight. The solution was filtered, layered with hexanes, and allowed to crystallize over several days yielding dark purple and pale green crystals. The crystalline products were identified as [K(2,2,2-crypt)][Fe(2,2′-bipyridine)$(mes)_2$] (**2**, dark purple) and [K(2,2,2-crypt)][Fe$(mes)_3$]·C_6H_{12} (**3**, pale green). Species **2** was purified by redissolving the mixture of solids in pyridine, filtering, and layering the solution with toluene. This yielded 148 mg of compositionally pure dark purple crystalline [K(2,2,2-crypt)][Fe(2,2′-bipyridine)$(mes)_2$] (yield 30%). A powder X-ray diffraction pattern was obtained which matched the simulated diffraction pattern based on the single-crystal X-ray diffraction data (Supporting Information, Figure S2). Anal. Calcd for $FeC_{46}H_{66}N_4O_6K$: C, 63.78%; H, 7.69%; N, 6.47%. Found: C, 63.66%; H, 7.54%; N, 6.52%. IR (cm^{-1}): 613 (w) 639 (w), 681 (w), 688 (w), 708 (w), 733 (m), 754 (w), 799 (w), 831 (m), 847 (w), 932 (s), 949 (s), 965 (w), 1011 (m), 1029 (w), 1105 (vs), 1130 (s), 1210 (w), 1258 (s), 1275 (w), 1290 (m), 1356 (s), 1413 (w), 1434 (w), 1444 (m), 1478 (m), 1497 (m), 1537 (w), 1556 (w), 1563 (w), 1582 (w), 1608 (w). Raman (cm^{-1}): 242 (w), 366 (w), 377 (w), 414 (w), 431 (w), 478 (w), 539 (w), 573 (m), 607 (m), 617 (m), 670 (w), 742 (w), 984 (s), 1093 (m), 1141 (m), 1213 (s), 1349 (w), 1412 (m), 1477 (s), 1512 (s), 1521 (m), 1586 (m).

X-ray Diffraction. Single-crystal X-ray diffraction data were collected using an Enraf-Nonius Kappa-CCD diffractometer and a 95 mm CCD area detector with a graphite-monochromated molybdenum K_α source ($\lambda = 0.71073$ Å). Crystals were selected under Paratone-N oil before being mounted on fibers and positioned under a dinitrogen stream. Dinitrogen flow temperatures were controlled by an Oxford Cryosystems cryostream. Equivalent reflections were merged and diffraction patterns processed with the DENZO and SCALEPACK programs.[21] Structures were subsequently solved using direct methods, and refined on F^2 using the SHELXL 97−2 package.[22]

Transmission powder X-ray patterns were recorded using a Siemens D5000 diffractometer in modified Debye−Scherrer geometry equipped with an MBraun position sensitive detector. The instrument produced Cu $K_{\alpha 1}$ radiation ($\lambda = 1.54056$ Å) using a germanium monochromator and a standard Cu source. Data were recorded on samples in flame-sealed capillaries under dinitrogen. The capillaries were mounted on a goniometer head and aligned so that rotation occurred along the long central axis of the capillary. During a measurement the capillary was rotated at ~60 rpm to minimize any preferred orientation effects that might occur.

SQUID Magnetometry. Magnetic properties were measured on unanchored polycrystalline samples of **1** and **2** with a Quantum Design MPMS XL SQUID magnetometer. Because of the extreme air- and moisture-sensitivity of the complexes they were flame-sealed under vacuum in Suprasil tubes.

Sample **1** was cooled to 2 K in zero applied field, and the magnetic susceptibility was measured between 2 and 300 K in a 0.01 T applied field. The sample was subsequently field cooled to 2 K, and magnetic susceptibility measurements were collected upon warming at regular intervals in a 0.01 T field. The resulting zero-field cooled and field cooled results were virtually identical and have been merged. A diamagnetic correction of -0.000286 cm^3 mol^{-1}, obtained from tables of Pascal's constants,[23] has been applied to the measured molar magnetic susceptibility of **1**.

To distinguish the intrinsic susceptibility of **2** from that of ferromagnetic impurities, the magnetization of **2** was measured at five applied fields between 4 and 5 T after an initial zero-field cooling to 2 K. The sample was warmed to 302 K in small increments, and the magnetization measured at each step at the same five fields. The slope of the resulting linear plot of the molar magnetization as a function of applied field was used to obtain the molar magnetic susceptibility at each temperature. A diamagnetic correction of -0.000551 cm^3 mol^{-1}, obtained from tables of Pascal's constants,[23] has been applied to the measured molar magnetic susceptibility of **2**.

Mössbauer Measurements. The Mössbauer spectra of **1** and **2** were measured between 85 and 295 K in a Janis Supervaritemp cryostat with a constant-acceleration spectrometer which utilized a rhodium matrix cobalt-57 source and was calibrated at 295 K with α-iron powder. The Mössbauer spectral absorbers contained about 50 mg/cm^2 of powder mixed with boron nitride; the absorbers were prepared in an argon atmosphere and mounted in the cryostat under an atmosphere of dinitrogen. The relative statistical errors are ± 0.005 mm/s for the isomer shifts, δ, $\pm$ 0.01 mm/s for the quadrupole splittings, ΔE_Q, and line widths, Γ, and $\pm 0.3\%$

(20) Klose, A.; Solari, E.; Floriani, C.; Chiesi-Villa, A.; Rizzoli, C.; Re, N. *J. Am. Chem. Soc.* **1994**, *116*, 9123.

(21) Otwinowski, Z.; Minor, W. *Processing of X-ray Diffraction Data Collected in Oscillation Mode*; Academic Press: New York, 1997.

(22) (a) Sheldrick, G. M. *Acta Crystallogr.* **1990**, *A46*, 467. (b) Sheldrick, G. M. *SHELX97 - Programs for Crystal Structure Analysis*, Release 97-2; Institut für Anorganische Chemie der Universität Göttingen: Göttingen, Germany, 1998.

(23) Bain, G. A.; Berry, J. F. *J. Chem. Educ.* **2008**, *85*, 532.

Scheme 1. Synthesis of **1**

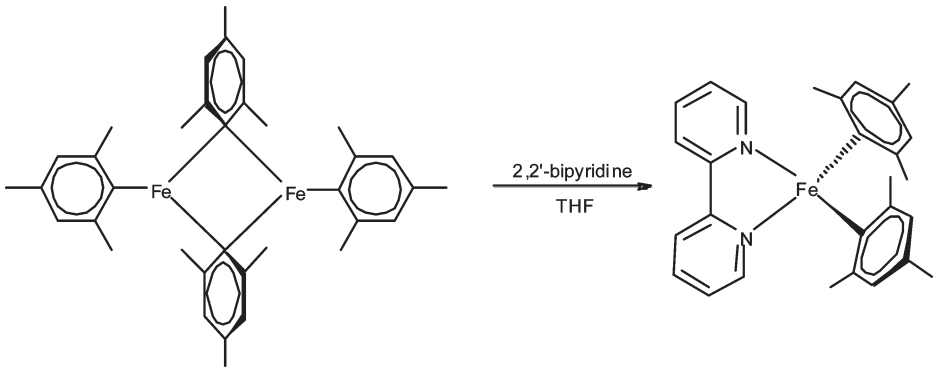

for the relative component areas; the absolute errors are approximately twice the statistical errors.

Computational Methods. All calculations described in this paper were performed using DFT as implemented in the ORCA program.[24] Unrestricted geometry optimizations on **1** and **2** were carried out using the B3LYP functional,[25] in combination with the TZVP basis set of Ahlrichs and co-workers on Fe and all coordinating atoms (N(1), N(2), C(11), C(21)),[26] and the SVP basis set elsewhere.[27] Initial atomic coordinates were taken from single-crystal X-ray diffraction experiments. Stationary points were confirmed to be minima by the absence of imaginary frequencies. For computation of the Mössbauer parameters of **1** and **2**, nonrelativistic single point calculations were carried out on the single-crystal X-ray structures using the B3LYP functional in combination with the CP(PPP) basis set for Fe and TZVP for nitrogen, carbon and hydrogen atoms.[28] The Mössbauer isomer shifts referenced to α-iron at room temperature were calculated from the computed electron densities at the iron center using the expression $\delta\,[\mathrm{mm/s}] = \alpha(\rho_0 - C) + \beta$ ($\alpha = -0.367 \pm 0.015$ (mm/s)/a_0^3, $\beta = 6.55 \pm 0.25$ mm/s and $C = 11800$ electrons/a_0^3, where a_0 is the Bohr radius) proposed by Neese and co-workers.[29]

Additional Characterization Techniques. IR data were recorded on solid samples in Nujol mulls. The mulls were made up inside an inert atmosphere glovebox and the KBr plates placed in an airtight container prior to data collection. Spectra were recorded on a Nicolet Magna-IR 560 spectrometer in absorbance mode (Happ-Genzel FT apodization) with a Ge/CsI beam splitter and liquid nitrogen cooled Mercury Cadmium Telluride (MCT) detector.

Raman spectra were recorded on solid samples under dinitrogen in flame-sealed Pyrex capillaries using a Dilor Labram 300 spectrometer. The excitation radiation was produced by a 20 mW helium−neon laser operating at a wavelength of 632.817 nm. Optical density filters could be inserted into the beam to reduce photon flux, decreasing the likelihood that photochemical reactions would take place during the measurement. Typically measurements were obtained at 0.1% of full intensity with a counting time of 100 s. Calibration of the spectrometer was performed before each measurement by referencing to the 520.7 nm line of a silicon wafer.

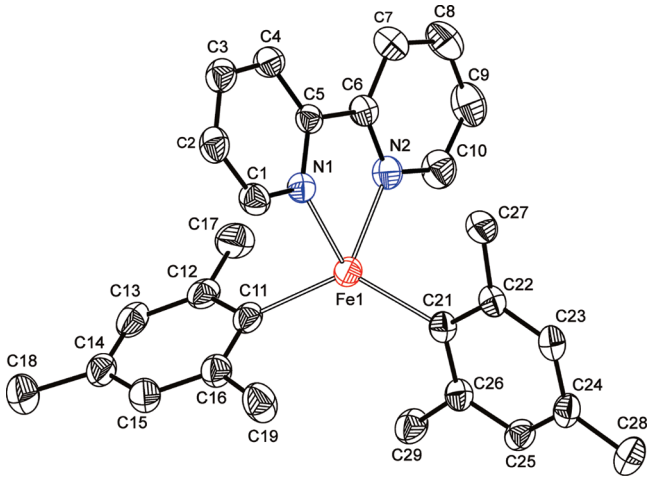

Figure 1. Thermal ellipsoid plot of the atoms in the asymmetric unit of **1** (hydrogen atoms have been omitted for clarity). Anisotropic displacement ellipsoids are pictured at the 50% probability level.

CW EPR experiments were performed using an X-band Bruker BioSpin GmbH EMX spectrometer equipped with a high sensitivity Bruker probehead and a low-temperature Oxford Instruments CF935 helium-flow cryostat. Experiments were conducted with 2−10 mW microwave power, 0.1 mT modulation amplitude, and a modulation frequency of 100 kHz. The magnetic field was calibrated at room temperature with an external 2,2-diphenyl-1-picrylhydrazyl standard ($g = 2.0036$). Solid state spectra were recorded on approximately 2 mg of sample in flame-sealed quartz capillaries.

Positive and negative ion mode electrospray mass spectra were recorded from *N*,*N*-dimethylformamide (DMF) solutions (10−20 μM) on a Masslynx LCT Time of Flight mass spectrometer with a Z-spray source (150 °C source temperature, 200 °C desolvation temperature, 2.4 kV capillary voltage and 25 V cone voltage). The samples were introduced directly with a 1 mL SGE syringe and a syringe pump at 0.6 mL/h.

CHN elemental analyses were performed on 5 mg samples submitted under vacuum in flame-sealed Pyrex ampules.

Results and Discussion

Synthesis. Complex **1** was synthesized by the direct reaction of 2,2′-bipyridine with $Fe_2(mes)_4$ in dry THF (Scheme 1) according to a modified procedure which has previously been employed as a versatile route toward $Fe(L\text{-}L)(mes)_2$ (where L-L represents a bidentate Lewis base).[30,31] A compositionally pure red crystalline solid can be obtained in high yields by layering a THF solution of **1** with hexane. Single-crystal X-ray diffraction

(24) Neese, F. *ORCA - an ab initio, density functional and semiempirical program package*, version 2.6, revision 35; University of Bonn: Bonn, Germany, Feb 2008 (http://www.thch.uni-bonn.de/tc/orca/).
(25) (a) Becke, A. D. *J. Chem. Phys.* **1993**, *98*, 5648. (b) Stevens, P. J.; Devlin, J. F.; Chabalowski, C. F.; Frisch, M. J. *J. Phys. Chem.* **1994**, *98*, 11623. (c) Lee, C.; Yang, W.; Parr, R. G. *Phys. Rev. B* **1988**, *37*, 785.
(26) Schäfer, A.; Huber, C.; Ahlrichs, R. *J. Chem. Phys.* **1994**, *100*, 5829.
(27) Schäfer, A.; Horn, H.; Ahlrichs, R. *J. Chem. Phys.* **1992**, *97*, 2571.
(28) Neese, F. *Inorg. Chim. Acta* **2002**, *337*, 181.
(29) Sinnecker, S.; Slep, L. D.; Bill, E.; Neese, F. *Inorg. Chem.* **2005**, *44*, 2245.

Table 1. Selected X-ray Data Collection and Refinement Parameters for [Fe(2,2′-bipyridine)(mes)$_2$] (**1**), [K(2,2,2-crypt)][Fe(2,2′-bipyridine)(mes)$_2$] (**2**), and [K(2,2,2-crypt)][Fe(mes)$_3$]·C_6H_{12} (**3**)

	1	2	3
formula	$C_{28}H_{30}FeN_2$	$C_{46}H_{66}FeKN_4O_6$	$C_{51}H_{81}FeKN_2O_6$
Fw	450.39	865.98	913.13
space group, Z	$P2(1)/c$, 4	$P2(1)2(1)2(1)$, 4	$C2/c$, 8
a (Å)	11.9696(2)	13.9644(1)	24.2771(2)
b (Å)	13.7989(3)	14.5989(1)	14.9508(1)
c (Å)	14.9180(3)	22.6777(2)	28.5112(3)
α (deg)	90.0	90.0	90.0
β (deg)	103.067(1)	90.0	97.664(1)
γ (deg)	90.0	90.0	90.0
V (Å^3)	2400.16(8)	4623.19(6)	10256.04(15)
ρ_{calc} (g cm^{-3})	1.246	1.244	1.183
radiation, λ (Å), temp (K)		Mo K_α, 0.71073, 150	
μ (mm^{-1})	0.645	0.466	0.422
reflections collected	10653	10530	17228
independent reflections	5454	10530	8901
R(int)	0.0302	0.0530	0.0276
R1/wR2,[a] $I \geq 2\sigma_I$ (%)	4.10/10.14	3.00/6.67	5.53/14.80
R1/wR2,[a] all data (%)	6.36/11.30	3.77/7.03	6.88/15.52

[a] $R1 = \sum||F_o| - |F_c||/\sum|F_o|$; $wR2 = \{\sum w(F_o^2 - F_c^2)^2/\sum w(F_o^2)^2\}^{1/2}$; $w = [\sigma^2(F_o)^2 + (AP)^2 + BP]^{-1}$, where $P = [(F_o)^2 + 2(F_c)^2]/3$ and the A and B values are 0.0580 and 0.63 for **1**, 0.0339 and 1.00 for **2**, and 0.0775 and 11.71 for **3**.

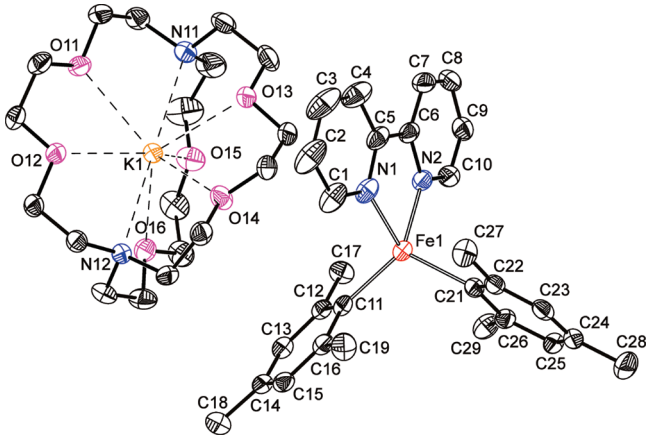

Figure 2. Thermal ellipsoid plot of the atoms in the asymmetric unit of **2** (hydrogen atoms have been omitted for clarity). Anisotropic displacement ellipsoids are pictured at the 50% probability level.

measurements confirmed that the iron(II) center adopts a distorted tetrahedral geometry with a chelating 2,2′-bipyridine ligand and two mesityl functionalities (pseudo-C_{2v}, Figure 1). Crystallographic data and experimental parameters for the structure are presented in Table 1. The purity of **1** was confirmed by powder X-ray diffraction (see Supporting Information and elemental analysis).

Reduction of **1** with potassium metal in THF in the presence of 2,2,2-crypt was found to yield a dark purple solution from which two complexes were isolated. The first and most abundant product, the result of a single electron reduction of the neutral parent compound, contains the [Fe(2,2′-bipyridyl)(mes)$_2$]$^{\bullet-}$ anion accompanied in the lattice by a [K(2,2,2-crypt)]$^+$ counter-cation (Figure 2). The anion exhibits a very similar distorted tetrahedral structure to that of complex **1**. A comparison of bond metric parameters for samples **1** and **2** is provided in Table 2.

A second crystalline product, characterized as the trigonal planar trismesityl adduct [K(2,2,2-crypt)][Fe(mes)$_3$]·C_6H_{12} (**3**, Figure 3), was also isolated from solution. The anionic [Fe(mes)$_3$]$^-$ moiety is isoelectronic with the known neutral complex Fe(col)(mes)$_2$ (col = 2,4,6-trimethylpyridine).[31] The non-stoichiometric relationship between complex **1** and **3** indicates that formation of **3** must be accompanied by an additional decomposition product, presumably a homoleptic 2,2′-bipyridyl complex such as [K(2,2,2-crypt)][Fe(2,2′-bipyridine)$_3$] (**4**). So far we have been unable to isolate **4**, although we did isolate a highly disordered crystalline phase of K[Fe(2,2′-bipyridine)$_3$]·2en (**5**) when the reduction of **1** was carried out in ethylenediamine with a stoichiometric deficiency of 2,2,2-crypt (Supporting Information, Figure S3). However, the crystallographic data obtained for sample **5** are not of sufficient quality to justify a detailed discussion of bond metric parameters.

Dissolution of a mixture of products **2** and **3** in pyridine followed by filtration and precipitation employing toluene was found to yield a pure sample of **2** in good yields relative to the $Fe_2(mes)_4$ starting material. Compositional purity of the solid sample was confirmed by elemental analysis and powder X-ray diffraction (see Supporting Information). The vibrational spectra of **2** are characteristic of a species in which the 2,2′-bipyridyl ligand is reduced: the IR spectrum reveals a strong ring deformation band at 949 cm^{-1}, as well as bands at 1497, 1532, and 1563 cm^{-1}, all of which were described by Nakamoto and co-workers as diagnostic of low valent bipyridyl metal complexes in which the ligand is believed to exist as a ligand radical.[16a]

Bond Metric Data. Complexes **1** and **2** both exhibit a distorted pseudo-tetrahedral coordination geometry around the iron(II) center, with angles of 70.2 and 78.6° between the planes defined by atoms Fe(1), N(1), and N(2) and Fe(1), C(11), and C(21) for **1** and **2**, respectively. The most significant differences between the two complexes are apparent in the Fe−N distances, which are

(30) (a) Magill, C. P.; Floriani, C.; Chiesi-Villa, A.; Rizzoli, C. *Inorg. Chem.* **1994**, *33*, 1928. (b) Müller, H.; Seidel, W.; Görls, H. *Z. Anorg. Allg. Chem.* **1996**, *622*, 756. (c) Hawrelak, E. J.; Bernskoetter, W. H.; Lobkovsky, E.; Yee, G. T.; Bill, E.; Chirik, P. J. *Inorg. Chem.* **2005**, *44*, 3103.

(31) Müller, H.; Seidel, W.; Görls, H. *Z. Anorg. Allg. Chem.* **1996**, *622*, 1269.

Table 2. Selected Bond Lengths (Å) and Angles (deg) of Complexes **1** and **2**[a]

parameter	**1**	$\mathbf{1}_{calc}$	**2**	$^{4}\mathbf{2}_{calc}$	$^{6}\mathbf{2}_{calc}$
Fe(1)−N(1)	2.156(2)	2.20	2.0897(15)	2.13	2.18
Fe(1)−N(2)	2.154(2)	2.20	2.0842(15)	2.13	2.18
Fe(1)−C(11)	2.087(2)	2.09	2.1029(17)	2.14	2.14
Fe(1)−C(21)	2.083(2)	2.09	2.0949(16)	2.14	2.14
C(5)−C(6)	1.481(3)	1.48	1.418(3)	1.43	1.43
N(1)−Fe(1)−N(2)	75.14(16)	74.1	77.00(6)	76.3	75.9
N(1)−Fe(1)−C(11)	95.54(7)	100.8	109.53(6)	104.7	104.0
N(1)−Fe(1)−C(21)	122.34(7)	125.6	119.99(6)	123.0	123.1
N(2)−Fe(1)−C(11)	122.31(8)	125.3	124.32(6)	123.0	123.1
N(2)−Fe(1)−C(21)	104.04(7)	99.9	108.35(6)	103.8	103.0
C(11)−Fe(1)−C(22)	126.74(8)	123.2	113.56(6)	119.5	120.8
angle between C−Fe−C and N−Fe−N planes (deg)	70.2	67.8	78.6	73.8	73.0
ρ Fe/2,2′-bipy		3.73		3.74/−0.86	3.79/1.07
$\langle S^2 \rangle$		6.05		4.62	8.78

[a] Both experimental and computed data are shown for comparison. For the computed structures ($\mathbf{1}_{calc}$, $^{4}\mathbf{2}_{calc}$, and $^{6}\mathbf{2}_{calc}$) the expectation value of the square of the total spin angular momentum operator ($\langle S^2 \rangle$) and Mulliken spin populations (ρ) on the iron center and the 2,2′-bipy ligand are also given.

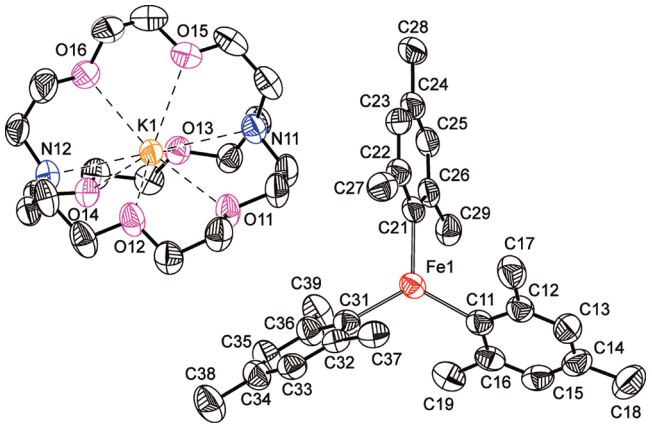

Figure 3. Thermal ellipsoid plot of the atoms in the asymmetric unit of **3** (cyclohexane solvent molecule and hydrogen atoms have been omitted for clarity). Anisotropic displacement ellipsoids are pictured at the 50% probability level.

some 0.06−0.07 Å shorter in **2**, and in the C−C bond between pyridine rings (Table 3) which contracts from 1.481(3) Å in **1** to 1.418(3) Å in **2**. The degree of contraction of this C−C bond is very similar to that observed in recent studies on the reduction of bipyridine to the corresponding anion and dianion.[32,33] The LUMO of 2,2′-bipyridyl, which becomes occupied upon reduction, is a π^* antibonding orbital with an in-phase relationship between the p orbitals on the carbon atoms linking the two rings (as pictured in Figure 4b). This in-phase relationship implies a greater degree of double bond character in the reduced species.

The crystal structure of sample **3** contains an $[Fe(mes)_3]^-$ anion in the asymmetric unit alongside a $[K(2,2,2\text{-crypt})]^+$ cation and a cyclohexane solvent molecule. The $[Fe(mes)_3]^-$ anion has a trigonal planar geometry with pseudo D_{3h} symmetry. The three iron−carbon bond lengths vary between 2.074(3) and 2.085(3) Å and are comparable to those present in complexes **1** (2.085(av) Å) and **2** (2.099(av) Å) and in other iron(II) organometallic complexes with aryl substituents.[30,31]

(32) Denning, M. S.; Irwin, M.; Goicoechea, J. M. *Inorg. Chem.* **2008**, *47*, 6118.
(33) Gore-Randall, E.; Irwin, M.; Denning, M. S.; Goicoechea, J. M. *Inorg. Chem.* **2009**, *48*, 8304.

Table 3. Bond Lengths (Å) of the 2,2′-Bipyridine Moieties in 2,2′-Bipyridine, the 2,2′-Bipyridyl Radical Anion,[33] Complexes **1** and **2**, and the Optimized Computed Structures

bond[a]	2,2′-bipy	2,2′-bipy$^{\bullet-}$	**1**	$\mathbf{1}_{calc}$	**2**	$^{4}\mathbf{2}_{calc}$	$^{6}\mathbf{2}_{calc}$
1	1.490(3)	1.430(av)	1.481(3)	1.48	1.418(3)	1.43	1.43
2	1.346(2)	1.389(av)	1.356(3)	1.35	1.385(2)	1.39	1.39
			1.347(3)		1.386(2)		
3	1.341(2)	1.337(av)	1.345(3)	1.34	1.354(3)	1.35	1.34
			1.342(3)		1.357(2)		
4	1.384(2)	1.376(av)	1.378(4)	1.39	1.371(3)	1.39	1.39
			1.385(4)		1.372(3)		
5	1.383(3)	1.404(av)	1.377(4)	1.40	1.400(4)	1.42	1.42
			1.383(5)		1.400(3)		
6	1.385(2)	1.364(av)	1.382(4)	1.39	1.352(4)	1.38	1.38
			1.384(4)		1.365(3)		
7	1.394(2)	1.428(av)	1.389(4)	1.40	1.420(3)	1.43	1.43
			1.395(4)		1.417(3)		

[a] Bond numbering scheme, as defined in Figure 4a.

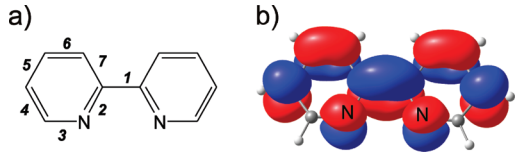

Figure 4. (a) Numbering scheme used to define 2,2′-bipyridine bond data for all complexes, (b) LUMO of 2,2′-bipyridine.

As noted earlier, the population of the LUMO of 2,2′-bipyridine that is apparent from the contraction of the central C−C bond in **2** could, in principle, be rationalized by either of two limiting formulations of the reduced species: a one-electron reduction of the ligand leading to a radical species, $[Fe^{II}(2,2'\text{-bipyridine}^{\bullet-})(mes)_2]^-$ or alternatively, metal-based reduction giving an iron(I) species, $[Fe^{I}(2,2'\text{-bipyridine})(mes)_2]^-$ with strong metal-to-ligand backbonding. To distinguish these two possibilities, we have analyzed the electronic structure of both the neutral and the reduced species using DFT. The neutral complex ($\mathbf{1}_{calc}$) has a quintet ground state and a highly distorted pseudo-tetrahedral coordination geometry around the iron(II) ion. The important structural features of the coordination sphere around the metal center are well reproduced by the calculations, with C−C, C−N, and Fe−C bond distances within ±0.01 Å of their crystallographic counterparts. The Fe−N distances are overestimated

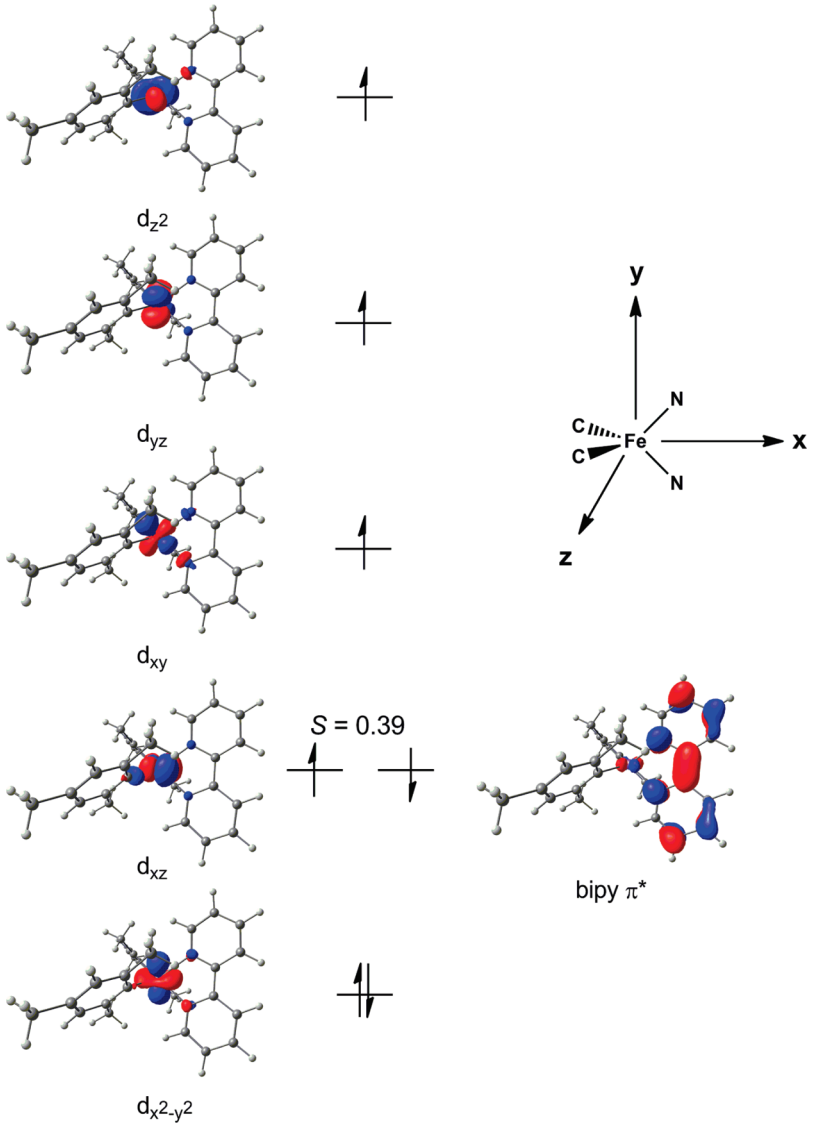

Figure 5. Spin-α and spin-β corresponding orbitals for the M_S = 3/2 broken-symmetry state of **2**.

by ~0.04 Å, errors that are typical of calculations performed with the B3LYP functional. Analysis of the electronic structure of **1** reveals an electronic distribution typical of a high-spin iron(II) ion, with a Mulliken spin density of 3.73 electrons on the metal and negligible elsewhere. For the anionic complex **2**, we have identified two distinct electronic states, a broken-symmetry quartet (M_S = 3/2), ^{4}**2**$_{\mathbf{calc}}$ and a sextet, ^{6}**2**$_{\mathbf{calc}}$, both of which contain localized electron distributions characteristic of iron(II) and 2,2′-bipy$^{\bullet-}$ groups. Thus, in the more stable quartet state, the Mulliken spin density on the iron(II) center (3.74) is essentially unchanged from that in **1**$_{\mathbf{calc}}$, while an unpaired electron of opposite spin is now located on the bipyridyl ligand (Mulliken spin density −0.86). Strong spin contamination is apparent in an $\langle S^2 \rangle$ value of 4.62 that greatly exceeds that of a pure quartet ($\langle S^2 \rangle$ = $S(S+1)$ = 3.75) and approaches the limit anticipated for completely localized antiferromagnetically coupled S_{Fe} = 2 and S_{bipy} = 1/2 radicals ($\langle S^2 \rangle$ = $S(S+1)$ + 1 = 4.75). The corresponding orbitals of ^{4}**2**$_{\mathbf{calc}}$ are summarized in Figure 5: the spin-α components of all five metal-based d orbitals are occupied, as is the spin-β component of one ($d_{x^2-y^2}$ in the coordinate system defined in Figure 5), giving a high-spin quintet configuration at the iron center. In contrast, only the spin-β component of the 2,2′-bipy LUMO is occupied. The spatial overlaps between corresponding spin-α and spin-β orbitals are all unity except for the d_{xz}/bipy LUMO pair where S = 0.39. The deviation from zero is characteristic of antiferromagnetic coupling, and arises from the tails on the ligand and metal in the spin-α and spin-β components shown in Figure 5, respectively. Although the reduction event can primarily be viewed as being ligand based, it still has a significant impact on the iron coordination sphere, most notably the Fe−C bonds, which are somewhat longer in **2** than **1**. These structural changes are a consequence of the Fe−C σ antibonding character of the d_{xz} orbital which accepts electron density from the 2,2′-bipy π^* orbital in **2**. In the related sextet S = 5/2 state (^{6}**2**$_{\mathbf{calc}}$), the basic features of the structure and Mulliken spin populations are very similar to those in ^{4}**2**$_{\mathbf{calc}}$, the major difference being that the unpaired electrons on the iron(II) center and the 2,2′-bipy ligand are aligned parallel to each other. The adiabatic separation between the two states is 3.9 kcal mol^{-1}, corresponding to

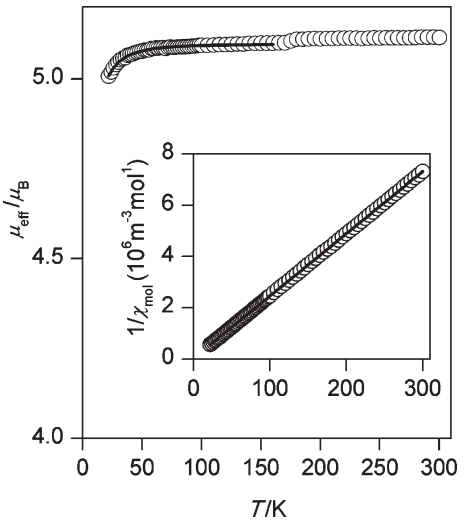

Figure 6. Temperature dependence between 2 to 300 K of the effective magnetic moment, μ_{eff}, of **1** obtained in a 0.01 T applied magnetic field (the full line corresponds to a fit of the zero-field splitting behavior of **1** between 20 and 160 K). Inset: The temperature dependence of $1/\chi_{mol}$ (the full line corresponds to a Curie−Weiss fit of the data between 20 and 300 K).

an exchange coupling constant, J, of $-328\ cm^{-1}$ (computed through the Yamaguchi formula ($J = -(E_{HS} - E_{BS})/(\langle S^2\rangle_{HS} - \langle S^2\rangle_{BS})$). The value of J indicates that exchange coupling is antiferromagnetic, but is not as strong as in related ferrous complexes of α-diimine and iminopyridine radicals studied by Wieghardt and co-workers, where values lie between -440 and $-630\ cm^{-1}$.[34] The rather weaker coupling in **2** probably has the same origins as the elongation of the Fe−C bonds noted above: the key metal-based d_{xz} orbital is also antibonding with respect to the very strong σ-donor mesityl groups, and so exchange coupling and Fe−C bonding are antagonistic. Finally, we note that despite extensive efforts using initial guess densities with different degrees of spin polarization, we have been unable to locate an alternative stable minimum for **2** corresponding to the $[Fe^{I}(2,2'\text{-bipyridine})(mes)_2]^-$ form. Additional details of the computational studies performed can be found in the Supporting Information.

SQUID Magnetometry. Sample **1** was cooled to 2 K in zero field, and the magnetic susceptibility measured between 2 and 300 K in an applied field of 0.01 T. The sample was subsequently cooled to 2 K in a 0.01 T field, and the magnetic susceptibility was measured upon warming to 300 K. The zero-field cooled (ZFC) and field cooled (FC) results were virtually identical and have been merged; the resulting effective magnetic moment, μ_{eff}, and the inverse molar magnetic susceptibility, $1/\chi_{mol}$, of **1** are shown in Figure 6. The results below 20 K have not been fitted because the data show some evidence of corruption because of poor sample centering. Between 20 and 300 K the inverse molar magnetic susceptibility of **1** exhibits Curie−Weiss behavior ($\chi_{mol} = N_A\mu_0{\mu_B}^2 S(S+1)g^2/3k(T-\Theta)$) with $g = 2.09$ and a Weiss temperature of -0.91 K for $S = 2$. The magnetic properties of **1** observed between 20 and 300 K correspond to a fully paramagnetic high-spin iron(II) complex with a small orbital contribution that increases μ_{eff} to $5.12\ \mu_B$, slightly more than the spin-only moment of $4.90\ \mu_B$. The decrease in μ_{eff} observed below about 50 K is the result of zero-field splitting of the iron(II) ground state by the low-symmetry of the coordination environment of **1**. The small increase in μ_{eff} observed at about 175 K is the result of a slight partial reorientation of the unanchored polycrystalline sample by the applied field on warming after both zero-field and field cooling. A fit between 20 and 160 K of the experimental data to the Zeeman plus ZFS spin Hamiltonian:

$$\hat{H} = \mathbf{S}\cdot\mathbf{D}\cdot\mathbf{S} + \mu_B\mathbf{B}\cdot\mathbf{g}\cdot\mathbf{S}$$

where the magnetic anisotropy of iron(II) is represented by the traceless tensor **D** results in an axial single-ion ZFS parameter $|D_{Fe}| = 6.7\ cm^{-1}$ and $g = 2.08$. Both the g and D values are typical for the distorted iron(II) coordination environment of **1**. From the results shown in Figure 6, it may be concluded that **1** exhibits the magnetic properties expected of a normal pseudo-tetrahedral iron(II) complex.

The collection of magnetic data for sample **2** was hindered by the presence of trace amounts (ppm levels) of an adventitious magnetic impurity in the sample. Although the compositional purity of **2** was confirmed by elemental analysis and powder X-ray diffraction, the substantially more sensitive SQUID susceptibility measurements indicate the presence of a trace of an unidentified ferromagnetic impurity. Two main factors support this hypothesis: first, a hysteresis in the FC and ZFC susceptibility measurements is apparent at low fields (0.1−0.5 T) but is saturated above 3.5 T (as evidenced by a scan of magnetization as a function of field). Second, the measured susceptibility values for **2** at low fields are abnormally high and vary from one sample to another, suggesting that this enhanced magnetic response arises from an external contaminant and not from the sample itself. Successive recrystallizations were found to decrease the concentration of the impurity and thus of its contribution to the bulk magnetization at low fields, but all attempts to remove this species completely have been unsuccessful thus far. We therefore conclude that the concentration of this contaminant must be below the detection limits of the bulk characterization techniques or the Mössbauer spectrometer (ca. 2 wt% detection limit), but at the same time large enough to allow its strong magnetic response to overwhelm the intrinsic magnetic properties of **2** at low fields. To separate the contribution of the ferromagnetic impurity from the intrinsic magnetization of **2**, the susceptibility of the sample was measured at five fields between 4 and 5 T for a given temperature, following an initial zero-field cooling to 2 K. The high fields saturate the magnetic response of the impurity, and the slope of the resulting linear plot of the molar magnetization as a function of applied field was used to obtain the molar magnetic susceptibility at a given temperature.

The temperature dependence of the molar susceptibility, χ_{mol}, and effective magnetic moment, μ_{eff}, for **2** are shown in Figure 7. For an exchange coupled complex of

(34) (a) Muresan, N.; Lu, C. C.; Ghosh, M.; Peters, J. C.; Abe, M.; Henling, L. M.; Weyhermüller, T.; Bill, E.; Wieghardt, K. *Inorg. Chem.* **2008**, *47*, 4579. (b) Bart, S. C.; Chopek, K.; Bill, E.; Bouwkamp, M. W.; Lobkovsky, E.; Neese, F.; Wieghardt, K.; Chirik, P. J. *J. Am. Chem. Soc.* **2006**, *128*, 13901.

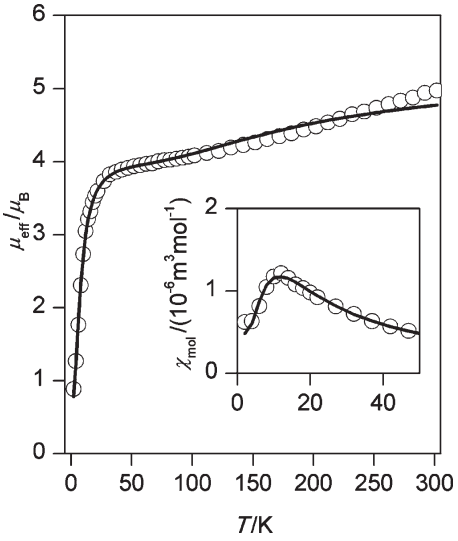

Figure 7. Temperature dependence of the effective magnetic moment, μ_{eff}, (calculated from differential susceptibility at B = 4.5 T) for complex **2** between 2 to 302 K. Inset: low-temperature region of χ_{mol}. Circles, experimental points; lines, calculated data using $J = -46.2$ cm^{-1}, $D_{Fe} = -10.6$ cm^{-1}, $g_{Fe} = 2.05$.

iron(II), $S_{Fe} = 2$, and the 2,2′-bipyridyl radical anion, $S_{bipy} = 1/2$, we can identify three distinct limiting cases: if the spins are ferromagnetically coupled then $S_{total} = 5/2$ and $\mu_{eff} = g[(S_{total})(S_{total} + 1)]^{1/2} = 5.92\,\mu_B$, while strong antiferromagnetic coupling gives $S_{total} = 3/2$ and a spin-only magnetic moment of $3.87\,\mu_B$. In the limit that the two spin systems are non-interacting, their contributions should be additive ($\chi_{total} = \chi_1 + \chi_2$), and $\mu_{eff} = (\mu_1^2 + \mu_2^2)^{1/2}$ $\mu_B = 5.20\,\mu_B$. In the temperature range 30−100 K the μ_{eff} of $\sim 3.8\,\mu_B$ is characteristic of an $S = 3/2$ ground state, but the increase in μ_{eff} above 100 K is rather more difficult to explain. The susceptibility can be fit to a spin Hamiltonian of the form:

$$\hat{H} = -2J(\mathbf{S}_{Fe}\cdot\mathbf{S}_{bipy}) + \sum_{i=1}^{2}\mathbf{S}_i\cdot\mathbf{D}\cdot\mathbf{S}_i + \mu_B\sum_{i=1}^{2}\mathbf{B}\cdot\mathbf{g}_i\cdot\mathbf{S}_i$$

where $S_{Fe} = 2$ and $S_{bipy} = 1/2$, using the following differential equation for the molar susceptibility:

$$\chi_{a,mol} = \mu_0 N_A kT\frac{\partial^2 \ln Z}{\partial B_a^2}$$

where Z is the partition function resulting from the diagonalization of the final spin matrices for a given orientation of the magnetic field B_a (where $a = x$ or z). The powder susceptibility was calculated as $\chi_{mol} = (\chi_{z,mol} + 2\chi_{x,mol})/3$ and the fitting procedure resulted in optimal values of $g_{Fe} = 2.05$, $J = -46.2$ cm^{-1}, and $D_{Fe} = -10.6$ cm^{-1} using fixed values of $g_{bipy} = 2.0$ and $D_{bipy} = 0$ for 2,2′-bipyridyl radical. With the best fit Heisenberg exchange constant of -46.2 cm^{-1}, the sextet state lies ~ 250 cm^{-1} ($5J$) above the ground state quartet and is significantly populated at higher temperatures. In contrast, the computed value of -328 cm^{-1} suggests that the sextet should remain unpopulated even at the highest accessible temperatures. It is possible that this discrepancy reflects the limitations of the theoretical method, but it is difficult to calibrate the methodology simply because in the majority

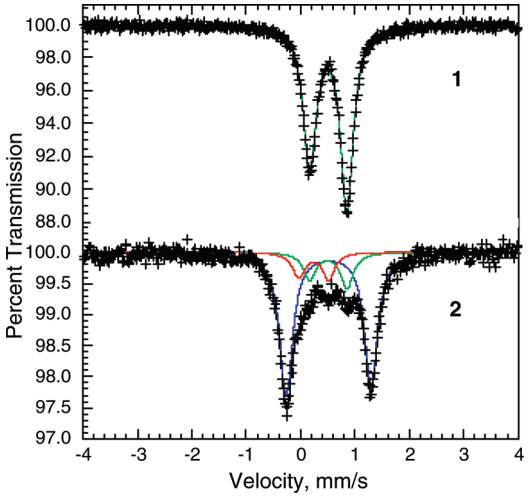

Figure 8. Mössbauer spectra of **1** and **2** obtained at 85 K. The green lines correspond to the neutral complex, **1**, the blue line corresponds to the reduced complex, **2**, and the red line corresponds to a small amount of paramagnetic high-spin iron(III) impurity.

of related systems only the ground state is occupied over the temperature range of the experiment, affording only a lower limit to $|J|$.[9b] In one of the few cases where the measured μ_{eff} does show temperature dependence (a cobalt(II) complex), the apparent population of the excited state is similarly inconsistent with the large computed J of -794 cm^{-1},[9a] suggesting that DFT may indeed systematically overestimate the magnitude of the exchange coupling in this class of system.[35] Despite the discrepancy in computed and experimental values of J for **2**, it is clear that both approaches are consistent in suggesting that the exchange coupling is considerably weaker in **2** than in comparable systems where strong σ-donor ligands such as mesityl are absent.[34]

Mössbauer Spectra. The iron-57 Mössbauer spectra of **1** and **2** were measured between 85 and 295 K (the 85 K spectra are shown in Figure 8). In agreement with the structural studies reported above, the spectra indicate that **1** is a paramagnetic high-spin iron(II) complex with a pseudo-tetrahedral coordination environment. The difference in the areas of the two components of the observed quadrupole doublet arises as a result of textural anisotropy in the absorber which is a consequence of the needle-like morphology of the crystals. The spectra have been fit with a quadrupole doublet with one single line width but with different component areas. The resulting hyperfine parameters are given in Table 4.

The isomer shifts of 0.511 to 0.406 mm/s observed for **1** between 85 and 295 K are slightly lower than expected for most pseudo-tetrahedral iron(II) complexes,[36−38] a lowering which may arise as a result of the strong σ-donor

(35) We note that it is also possible to fit the susceptibility of **2** to a spin Hamiltonian involving an isolated $S = 3/2$ state (effectively assuming infinite J), in which case the rise in χ_{mol} at high temperatures can only be reproduced by invoking a large temperature independent contribution (see Supporting Information).

(36) Reiff, W. M.; Long, G. J. In *Mössbauer Spectroscopy Applied to Inorganic Chemistry*; Long, G. J., Ed.; Plenum Press: New York, 1984, Vol. *1*, pp 245−285.

(37) Vogel, C.; Heinemann, F. W.; Sutter, J.; Anthon, C.; Meyer, K. *Angew. Chem., Int. Ed.* **2008**, *47*, 1.

(38) Scott, T. A.; Berlinguette, C. P.; Holm, R. H.; Zhou, H.-C. *Proc. Nat. Acad. Sci.* **2005**, *102*, 9741.

Table 4. Mössbauer Spectral Parameters of **1** and **2**

complex	T, K	δ, mm/s[a]	ΔE_Q, mm/s	Γ, mm/s	area, %	normalized area, (%ε) (mm/s)/(mg Fe/cm^2)	assignment
1	295	0.406	0.62	0.28	100	0.00386	**1**
	255	0.425	0.63	0.25	100	0.00539	**1**
	225	0.441	0.64	0.26	100	0.00728	**1**
	155	0.481	0.67	0.25	100	0.0130	**1**
	85	0.511	0.69	0.28	100	0.0213	**1**
$\mathbf{1}_{calc}$		0.361	1.08[b]				
2	295	0.408	1.36	0.34	30.9	0.000294	**2**
		0.406	0.62	0.28	21.4	0.000204	**1**
		0.156	0.62	0.37	47.6	0.000453	high-spin iron(III)
	225	0.455	1.49	0.30	52.1	0.000728	**2**
		0.441	0.64	0.26	19.0	0.000312	**1**
		0.182	0.74	0.40	28.9	0.000478	high-spin iron(III)
	155	0.497	1.56	0.29	59.0	0.00142	**2**
		0.481	0.67	0.25	13.6	0.00033	**1**
		0.206	0.62	0.46	27.4	0.00066	high-spin iron(III)
	85	0.516	1.56	0.29	71.2	0.00256	**2**
		0.511	0.69	0.28	15.3	0.00055	**1**
		0.235	0.59	0.29	13.5	0.00048	high-spin iron(III)
$\mathbf{2}_{calc}$		0.395	2.05[b]				

[a] The isomer shifts are given relative to 295 K α-iron powder. [b] Calculated using the corresponding η value of 0.278 and 0.413 for $\mathbf{1}_{calc}$ and $^4\mathbf{2}_{calc}$, respectively.

character of the mesityl ligands. It is worth noting that there is evidence in the literature for other high-spin pseudo-tetrahedral iron(II) complexes with comparable shifts.[39] The temperature dependence of the isomer shift of **1**, see Figure 9, has been fit with the Debye model for a solid,[40] and the resulting Mössbauer temperature, Θ_M, of 462(38) K is consistent with the pseudo-tetrahedral coordination environment of **1**.[41] The quadrupole splitting, ΔE_Q, of about 0.65 mm/s observed for **1** is consistent with the distortion of the pseudo-tetrahedral iron(II) coordination environment but, unexpectedly, the ΔE_Q is almost independent of temperature between 85 and 295 K. A fit of ΔE_Q with the Ingalls' model for the temperature dependence of the valence contribution to the quadrupole splitting, Figure 9, indicates that the low-symmetry component of the pseudo-tetrahedral crystal field removes the degeneracy of the two 3d ground state e orbitals by 610(30) cm^{-1}, an orbital splitting that is reasonable for the observed distortion at the iron(II) site.

Because of the extreme air- and moisture-sensitivity of sample **2** the study of its Mössbauer spectra proved more complicated than for complex **1**. Well-resolved spectra of **2** were, however, obtained between 85 and 295 K (Figure 8), and at 85 K the spectrum exhibits a major quadrupole doublet, the blue component, corresponding to a tetrahedral iron(II) complex, as well as two minor components. Of these two components one has identical parameters to those observed for the starting material, **1** (green), and the second doublet exhibits parameters characteristic of a high-spin iron(III) decomposition product (red). At this point it is not possible to determine whether the iron(III) component is intrinsic to the preparation of **2** or if it is an artifact of preparing the

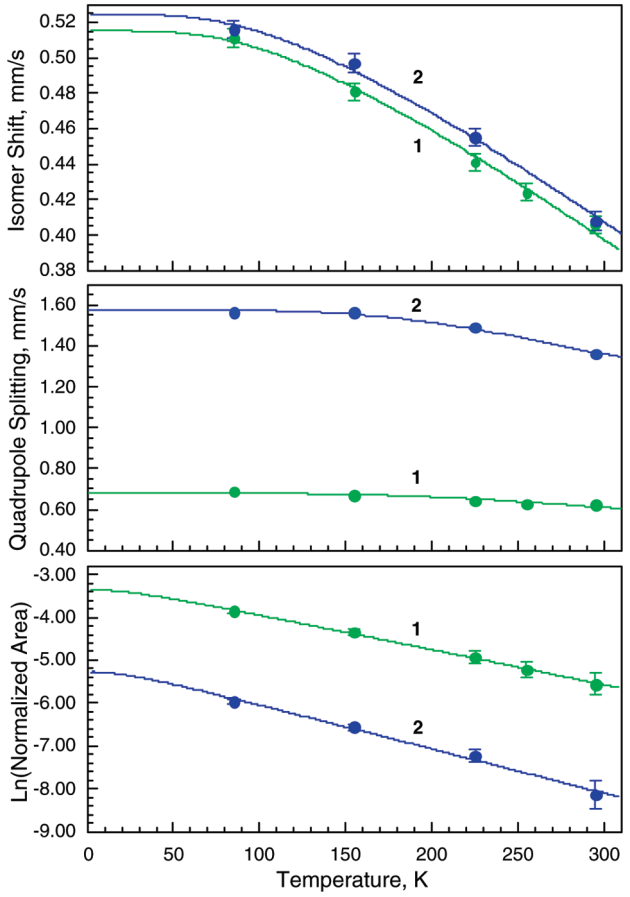

Figure 9. Temperature dependence of Mössbauer spectral parameters of the neutral complex, **1** (green) and the reduced complex, **2** (blue). Unless shown, the errors are no larger than the data points.

Mössbauer spectral absorber, but the latter possibility seems more likely (samples were very briefly exposed to air before being mounted on the spectrometer). The isomer shifts of 0.50 to 0.65 mm/s reported by Wieghardt for two related bis(α-diamine)iron(II) complexes at 80 K are similar to those of **2** (0.516 mm/s).[34] The temperature

(39) Khusniyarov, M. M.; Weyhermüller, T.; Bill, E.; Wieghardt, K. *J. Am. Chem. Soc.* **2009**, *131*, 1208.
(40) Shenoy, G. K.; Wagner, F. E.; Kalvius, G. M. In *Mössbauer Isomer Shifts*; Shenoy, G. K., Wagner, F. E., Eds.; Elsevier Science: North-Holland, Amsterdam, 1978; p 49.
(41) Owen, T.; Grandjean, F.; Long, G. J.; Domasevitch, K. V.; Gerasimchuk, N. *Inorg. Chem.* **2008**, *47*, 8704, and references reported therein.

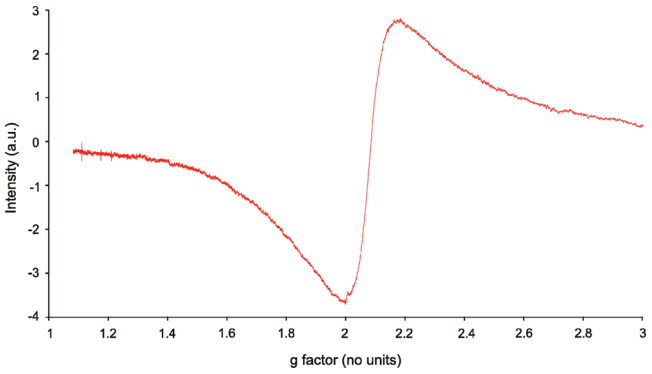

Figure 10. X-band (9.3896 GHz) CW EPR spectrum of a solid sample of **2** recorded at 296 K.

dependence of the isomer shift of **2** (Figure 9) has also been fit with the Debye model for a solid, and the resulting Θ_M is 466(40) K, a temperature that is identical to the 462(38) K observed for **1**. In contrast to the rather similar isomer shifts of **1** and **2**, their quadrupole splittings, ΔE_Q, are very different. An increase in ΔE_Q by a little more than a factor of 2 to 1.56 mm/s at 85 K is somewhat unexpected considering that there is little change in the iron(II) moiety on going from **1** to **2**, but computational studies (vide infra) indicate that these values are very sensitive to the immediate coordination environment of the iron(II) ion. On the basis of the Ingalls' model (Figure 9), the temperature dependence of ΔE_Q for **2** can be fit assuming a pseudo-tetrahedral crystal field that removes the degeneracy of the two 3d ground state e orbitals by 546(20) cm^{-1}, an orbital splitting that again is reasonable for the observed distortion at the iron(II) site and comparable to the 610(30) cm^{-1} splitting observed in **1**.

The principal reason for measuring the Mössbauer spectra of **2** was to determine whether the reduction of **1** to yield **2** led to a reduction either of the iron(II) ion or of the bipyridyl ligand, to form a $bipy^{\bullet-}$ radical anion,[33] and the answer appears to be unambiguous. The isomer shifts of the iron(II) ion in **2** are very similar to those observed in sample **1**, an observation that is apparently inconsistent with a change in metal oxidation state, eliminating the $[Fe^{I}(2,2'\text{-bipyridine})(mes)_2]^{-}$ valence tautomer. To further validate this conclusion we have computed the Mössbauer spectral hyperfine parameters (δ and ΔE_Q) for both **1** and ^{4}**2** (using the crystallographic geometries reported in Table 2), where our electronic structure analysis is unambiguous in confirming the iron(II) oxidation state in both cases. The computed electron densities, ρ_0, at the ^{57}Fe nucleus for **1** and ^{4}**2** are 11816.86 and 11816.76 electrons/a.u.^{3}, respectively, corresponding to isomer shifts of 0.361 and 0.395 mm/s using the linear regression curve δ [mm/s] = $\alpha(\rho_0 - C) + \beta$ ($\alpha = -0.367 \pm 0.015$ (mm/s)/a_0^3, $\beta = 6.55 \pm 0.25$ mm/s and $C = 11800$ electrons/a_0^3) proposed by Neese and co-workers.[29] Within the error limits imposed by the calibration process, the computed values of δ for **1** and ^{4}**2** are identical and consistent with the experimental data. The calculated principal component, V_{zz}, and the asymmetry parameter, η, of the electric field gradient tensor are 0.6538 au, 0.278 and 1.2288 au, 0.413 for **1** and ^{4}**2**, respectively. Using these values and the expression $\Delta E_Q = 1/2\ eQV_{zz}(1 + \eta^2/3)^{1/2}$, with a value of 0.16 barn for $Q(^{57}Fe)$ and a unit conversion of 1 au = 9.717×10^{21} V/m^2 = 1.617 mm/s, the trend in ΔE_Q is also reproduced with encouraging accuracy: ΔE_Q increases by a factor of 2 from 1.08 mm/s in **1** to 2.05 mm/s in ^{4}**2** compared to experimental values of 0.69 and 1.56 mm/s, respectively.

In principle, the large quadrupole splitting in **2** could arise from a more asymmetric arrangement of the primary coordination sphere, the presence of a strong π-donor 2,2′-bipy radical ligand, or a combination of the two. To distinguish these two distinct possibilities we have recomputed the Mössbauer hyperfine parameters of **1** using the geometry of ^{4}**2** and vice versa. At either geometry, the computed values of δ and ΔE_Q for the neutral and anionic species are almost indistinguishable, providing compelling evidence that the shifts in ΔE_Q from **1** to **2** are due to the apparently minor changes in geometry, and hence the σ framework (in particular the Fe−C bonds), and not directly to the presence or absence of an electron in the LUMO of the 2,2′-bipy ligand.

EPR. EPR spectra were recorded for samples **1** and **2**. A solid sample of **1** was found to give rise to a very weak resonance in its EPR spectrum at 4 K of comparable magnitude to sample cavity background signals. Sample **1** is expected to be EPR silent as the iron(II) nucleus in this complex is a non-Kramers ion ($S = 2$). The EPR spectrum of a solid sample of **2** reveals a much stronger resonance at room temperature with a g value of 2.086 (Figure 10). This resonance is relatively broad because of the coupling of the electron of the radical anion with the iron(II) center and/or fast relaxation effects. Variable temperature EPR measurements on this solid sample reveal that the resonance remains constant above 20 K, but below this point there is a dramatic sharpening of the signal (Supporting Information, Figure S13). This sharpening coincides with the maximum in the molar magnetic susceptibility observed for **2**. Similar phenomena have been observed for other complexes reported in the literature in which there is antiferromagnetic coupling between the unpaired electrons of a ligand radical and a transition metal center.[42] The EPR spectrum of **2** in a THF glass at 4.63 K reveals a sharp resonance with a g factor of 1.994.

Conclusions

We have carried out an extensive experimental and computational study on the one electron chemical reduction of Fe(2,2′-bipyridine)(mes)$_2$ (**1**) to yield [K(2,2,2-crypt)][Fe(2,2′-bipyridine)(mes)$_2$] (**2**). All available structural, magnetic and spectroscopic data indicate that the reduction results in the occupation of a π^* antibonding ligand-based orbital giving rise to an iron(II) complex of the 2,2′-bipyridyl radical anion, a conclusion that is strongly supported by DFT calculations. To the best of our knowledge **2** represents the first example of a fully characterized transition metal complex of this radical anion. The structural characteristics of the 2,2′-bipy ligand in **2** are similar to other complexes in the literature where the reduction has been assigned as a metal- rather than ligand-based event, and suggest that complexes of the $2,2'\text{-bipy}^{\bullet-}$ radical may be more common than previously suspected. We are currently involved in a series of studies aimed at the isolation of a coordination complex of the

(42) Benelli, C.; Gatteschi, D.; Zanchini, C.; Doedens, R. J.; Dickman, M. H.; Porter, L. C. *Inorg. Chem.* **1986**, *25*, 3453.

2,2′-bipyridyl dianion to observe the behavior of such a species toward a variety of substrates with the aim of exploiting the "non-innocent" behavior of this ubiquitous ligand.

Acknowledgment. J.M.G. acknowledges the EPSRC (EP/F00186X/1, PDRA MSD) and the University of Oxford (DTA studentship M.I.) for financial support of this research. J.E.M. acknowledges the EPSRC (EP/G002789/2). We also thank Steve Boyer (London Metropolitan University) for performing all elemental analyses and the Oxford Crystallographic Service, the Oxford Supercomputing Centre, and CAESR for access to instrumentation and Prof. R. Cloots and Mr. G. Toussaint for the use of their inert atmosphere drybox at the University of Liège. F.G. thanks the Fonds National de la Recherche Scientifique, Belgium (Grants 9.456595 and 1.5.064.05) for financial support.

Supporting Information Available: X-ray crystallographic file in CIF format (**1**, **2**, **3**). Powder X-ray patterns for samples **1** and **2**, single-crystal X-ray diffraction data for sample **5**, as well as details of computational studies, alternative fits for the magnetic data of **2**, and variable temperature EPR spectra. This material is available free of charge via the Internet at http://pubs.acs.org.